

Models for the magnetic ac susceptibility of granular superferromagnetic CoFe/Al₂O₃

O. Petracic,^{1,2,*} A. Glatz,^{3,4,†} and W. Kleemann²

¹*Physics Department, University of California, San Diego, La Jolla, California 92093*

²*Angewandte Physik, Universität Duisburg-Essen, 47048 Duisburg, Germany*

³*Materials Science Division, Argonne National Laboratory, Argonne, Illinois 60439*

⁴*Institut für Theoretische Physik, Universität zu Köln, 50937 Köln, Germany*

(Dated: February 2, 2008)

The magnetization and magnetic ac susceptibility, $\chi = \chi' - i\chi''$, of superferromagnetic systems are studied by numerical simulations. The Cole-Cole plot, χ'' vs. χ' , is used as a tool for classifying magnetic systems by their dynamical behavior. The simulations of the magnetization hysteresis and the ac susceptibility are performed with two approaches for a driven domain wall in random media. The studies are motivated by recent experimental results on the interacting nanoparticle system Co₈₀Fe₂₀/Al₂O₃ showing superferromagnetic behavior. Its Cole-Cole plot indicates domain wall motion dynamics similarly to a disordered ferromagnet, including pinning and sliding motion. With our models we can successfully reproduce the features found in the experimental Cole-Cole plots.

PACS numbers: 75.60.-d, 75.75.+a, 75.40.Gb, 75.40.Mg

I. INTRODUCTION

The physics of interacting ferromagnetic (FM) nanoparticles is a vivid topic of modern magnetism research. This also applies to the study of the reversal dynamics in thin FM films. The first subject, the properties of interacting FM nanoparticles, is investigated by many groups focusing either on the preparation (e.g., Ref. 1,2) or the magnetic properties (e.g. Refs. 1,3,4,5,6,7). Numerous theoretical studies were performed in order to understand the observed phenomena or to explore possible new effects (e.g. Refs. 8,9,10,11,12).

While individual single-domain FM nanoparticles exhibit superparamagnetic (SPM) behavior^{1,13,14,15}, interacting ensembles lead to very different kinds of phenomena depending on the type and strength of interactions. Dipolar interactions become relevant since the magnetic moment e.g. for particles with diameter 5 nm is of the order $5000\mu_B$, while the inter-particle distances are of the order $1 - 10$ nm. The simple formula for the mean dipolar energy of a particle to one neighbor, $E_{d-d}/k_B = (\mu_0/4\pi k_B)\mu^2/D^3$, yields already 16 K for $D = 10$ nm. Considering many neighbors and shorter distances it is obvious, that the effects of dipolar interaction can be observed even at temperatures of the order 100 K. In addition, several other types of interactions are proposed, i.e., higher order multipole terms of dipolar^{16,17}, tunneling exchange¹⁸ or even retarded van der Waals interactions¹⁹. Independent from the still open question which interactions are relevant, one can summarize, that essentially three different kinds of phenomena occur²⁰:

For large inter-particle distances, and hence a small concentration of particles, the (dipolar) interaction is only a perturbation to the individual particle behavior and no collective behavior is found.^{6,20,21} For intermediate concentrations a superspin glass (SSG) phase is encountered. In this case the particle moments (superspins)

collectively freeze into a spin glass phase below a critical temperature, T_g .^{4,20,22,23,24} For even higher concentrations a superferromagnetic (SFM) state is found. It is characterized by a ferromagnetic arrangement of the moments.^{25,26,27,28,29,30} The magnetic dynamic behavior resembles at the first glance that of the SSG case, but actually shows features of domain wall motion similar to an impure ferromagnet as will be discussed below.³¹ Here one should mention that also additional types of collective ordering are proposed in literature, e.g., the correlated superspin glass state (CSSG),^{32,33} and also that the effects of surface spin disorder may become significant.³⁴

The second topic, the reversal dynamics in thin ferromagnetic films finds equally large interest. Both experimental^{35,36} and theoretical^{35,37,38,39} investigations are performed in order to achieve a better understanding of the processes during the hysteresis cycle. The magnetization reversal occurs either by domain wall (DW) nucleation and motion or by magnetization rotation.⁴⁰ The DW motion at constant (dc) fields is characterized by three regions depending on the field strength, that is *creep*, *depinning*, and *sliding motion*. Creep is the thermally activated motion of DWs, where the average DW velocity is $v(H) \propto \exp[-(T_p/T)(H/H_p)^{-\mu}]$.^{41,42,43} This behavior is encountered at small applied fields, $H \ll H_p$, where H_p is the critical depinning threshold and T_p proportional to a characteristic depinning energy, $U_p = k_B T_p$. At zero temperature a dynamic phase transition of second order at $H = H_p$ is found. The mean DW velocity, v , can be interpreted as order parameter of the depinning transition, with $v(H) \propto (H - H_p)^\beta$.⁴⁴ At $T > 0$ the phase transition is smeared out and the $v(H)$ curve is rounded. Beyond the depinning region, $H \gg H_p$, sliding motion sets in and the DW velocity becomes linear with applied field, $v \approx \gamma H$. Here γ is the mobility coefficient.^{45,46}

In alternating (ac) (magnetic) fields, $H = H_0 \sin(\omega t)$, additional dynamical effects will arise. The coercive

field and the loop area become dependent on the frequency or in other words on the field sweep rate,^{36,39} dynamic phase transitions and crossovers occur,^{38,45,47} the ac susceptibility vs. temperature shows similar features as spin glass systems⁴⁸ and a DW velocity hysteresis is found.⁴⁹ Different models are employed, i.e., numerical solutions of the coupled differential equations of the DW displacement starting from Maxwell's equations³⁷, using an interface depinning model for an elastic DW in random media^{38,45,49,50} (sometimes referred to as quenched Edwards-Wilkinson⁵¹ (EW) equation), kinetic simulations of a DW in the sliding motion regime³⁹ and calculations based on Fatuzzo's domain theory⁵² applied to ultrathin magnetic layers.³⁵

In this paper we will present model investigations motivated by recent experiments on the SFM system [Co₈₀Fe₂₀(1.4 nm)/Al₂O₃(3 nm)]₁₀ being a realization of a densely packed ensemble of interacting nanoparticles. The complex magnetic ac susceptibility, $\chi' - i\chi''$, reveals that the magnetic dynamic behavior can be explained within the concept of domain wall motion in an impure ferromagnet.^{31,53} That means, the granular system behaves like a thin FM film, only with the difference, that the atomic moments are to be replaced by 'super-moments' of the individual particles. This concept implies that the FM nanoparticles remain single-domain whereas the ensemble shows collective SFM behavior. This idea is evidenced from the *Cole-Cole plot*, χ'' vs. χ' .⁵⁴ Hence we will focus on the Cole-Cole presentation and compare it to that found experimentally.

II. AC SUSCEPTIBILITY AND COLE-COLE PLOTS

Magnetic systems exhibiting relaxational phenomena can be characterized by the complex ac susceptibility, $\chi(\omega) = \chi' - i\chi''$. The time dependent complex ac susceptibility is defined as

$$M(t) = \tilde{\chi}(t)\tilde{H}(t), \quad (1)$$

with the *complex* external field $\tilde{H}(t) = -iH_0e^{i\omega t}$ [$H(t) = \text{Re}(\tilde{H}(t)) = H_0 \sin(\omega t)$] and the magnetization M . In this paper we study the time independent term of the Fourier series for $\tilde{\chi}(t)$, namely:

$$\chi \equiv \chi' - i\chi'' = \frac{1}{T} \int_0^T dt \tilde{\chi}(t), \quad (2)$$

with $T = 2\pi/\omega = 1/f$.

This defines χ' and χ'' as follows

$$\chi'(\omega) = \frac{1}{H_0 T} \int_0^T dt M(t) \sin(\omega t) \quad (3)$$

$$\chi''(\omega) = -\frac{1}{H_0 T} \int_0^T dt M(t) \cos(\omega t). \quad (4)$$

Or equivalently - if we define $\tilde{\chi}(t) = \frac{dM(t)}{dH(t)} = \dot{M}(t) \left(\frac{d\tilde{H}}{dt} \right)^{-1}$:

$$\chi'(\omega) = \frac{1}{2\pi H_0} \int_0^T dt \dot{M}(t) \cos(\omega t) \quad (5)$$

$$\chi''(\omega) = \frac{1}{2\pi H_0} \int_0^T dt \dot{M}(t) \sin(\omega t). \quad (6)$$

One way of presenting the data is the Cole-Cole or Argand representation. The imaginary part is plotted against the real part of the susceptibility, χ'' vs. χ' .^{54,55} It can serve as a fingerprint to distinguish different magnetic systems by their dynamic response. E.g. a monodisperse ensemble of non-interacting SPM particles has exactly one relaxation time, $\tau = \tau_0 \exp(KV/k_B T)$,^{13,14} and will display a semicircle with the center on the χ' -axis. Here K is an effective anisotropy constant, V the volume of the particle and τ_0 corresponds to the microscopic spin-flip time which is of order of 10^{-10} s. The Cole-Cole plot can easily be derived from an analytic expression for the ac susceptibility given in Ref. 8 for a monodisperse SPM ensemble in zero-field with a random distribution of anisotropy axis directions:

$$\chi'(\omega) = \mu_0 \frac{M_s^2}{3K} \left[1 + \frac{KV}{k_B T} \frac{1}{1 + (\omega\tau)^2} \right] \quad (7)$$

$$\chi''(\omega) = \mu_0 \frac{M_s^2}{3} \frac{V}{k_B T} \frac{\omega\tau}{1 + (\omega\tau)^2} \quad (8)$$

where M_s is the saturation value of the magnetization. Defining $\alpha \equiv \mu_0 M_s^2 / 3K$ and $\sigma \equiv KV/k_B T$ and eliminating ω one gets

$$\chi'' = \sqrt{\left(\frac{\alpha\sigma}{2} \right)^2 - \left(\chi' - \frac{\alpha(2+\sigma)}{2} \right)^2}, \quad (9)$$

which describes a circle with the radius $r = \alpha\sigma/2$ and center at $(\alpha(2+\sigma)/2; 0)$ in the Cole-Cole plane.

In Fig. 1(a) the result is shown for parameters $\mu_0 M_s^2 / 3K = 1$ and $KV/k_B T = 1$. In the case of a particle size distribution (polydispersivity) and hence a distribution of relaxation times the Cole-Cole semicircle is expected to become flattened and/or distorted.⁵⁵ Fig. 1(b)

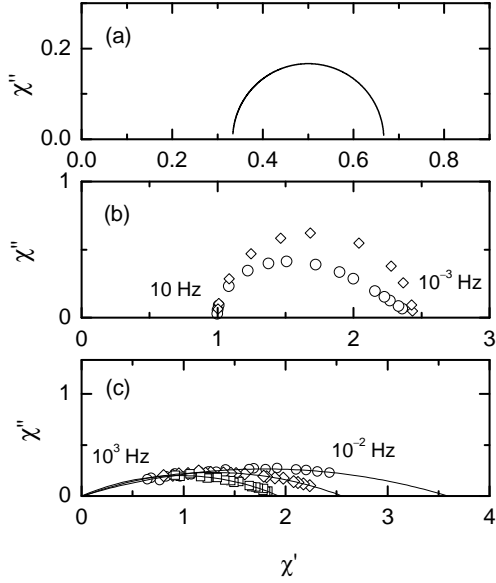


FIG. 1: Cole-Cole plots, χ'' vs. χ' , (a) analytically obtained for a non-interacting monodisperse ensemble of SPM particles with $\mu_0 M_s^2 / 3K = 1$ and $KV/k_B T = 1$ (see text), (b) numerical result for a polydisperse ensemble with a log-normal distribution (circles) and a Maxwell distribution (diamonds) of particle volumes with $\mu_0 M_s^2 / 3K = 1$, $K/k_B T = 1$, $\tau_0 = 1$, $\Delta V = 0.9$ and $\langle V \rangle = 1$, and (c) shows experimentally obtained curves on the SSG system [CoFe(0.9 nm)/Al₂O₃(3 nm)]₁₀ at three different temperatures, $T = 50, 55$ and 60 K (Ref. 57). The particle sizes follow a Gaussian distribution with $\langle V \rangle = 11.5$ nm³ and $\Delta V = 0.95$ nm³. The frequency range is indicated in the figure.

shows two numerically obtained curves, where a particle volume distribution from a log-normal distribution (circles) and a Maxwell distribution⁶¹ (diamonds) is assumed using $\mu_0 M_s^2 / 3K = 1$, $K/k_B T = 1$, $\tau_0 = 1$, $\langle V \rangle = 1$ and a relatively broad distribution width $\Delta V = 0.9$. One finds an asymmetric Cole-Cole plot for the case of a log-normal distribution. Obviously this is due to the asymmetry of the distribution itself. By choosing the more symmetric Maxwell distribution the curve becomes symmetric and only slightly shifted downward. Extremely high polydispersity is found in spin glass systems, where the distribution of relaxation times is expected to become infinitely broad due to collective behavior.⁵⁶ Fig. 1(c) shows an experimentally obtained Cole-Cole plot on the SSG system [Co₈₀Fe₂₀(0.9 nm)/ Al₂O₃(3 nm)]₁₀ at different temperatures, $T = 50, 55$ and 60 K.⁵⁷ Here the particle sizes follow a relatively narrow Gaussian distribution with $\langle V \rangle = 11.5$ nm³ and $\Delta V = 0.95$ nm³ as evidenced from a transmission electron microscopy image for a similar sample.⁷

III. MODELS

We study the complex ac susceptibility with two different approaches, where account is taken of the fact, that M is controlled by the field-induced sideways motion of one DW. In this case it follows that $\dot{M}(t) \propto v(t)$, where $v(t)$ is the (mean) DW velocity, being a function of the external field $H(t)$ and temperature T . Both approaches are based on the same underlying model for a d -dimensional elastic DW in a $D = (d + 1)$ -dimensional random environment:

$$\mathcal{H} = \int d^d x \left\{ \frac{\Gamma}{2} (\nabla_{\mathbf{x}} Z)^2 - H(t)Z + V_R(\mathbf{x}, Z) \right\}, \quad (10)$$

where $Z = Z(\mathbf{x}, t)$ is the d -dimensional displacement profile of the DW with internal coordinate \mathbf{x} , Γ the stiffness of the DW, and V_R the (quenched) random potential. V_R can be written in the following way:

$$V_R[\mathbf{x}, Z(\mathbf{x}, t)] = - \int_0^Z d\tilde{Z} g[\mathbf{x}, \tilde{Z}(\mathbf{x}, t)], \quad (11)$$

where $g[\mathbf{x}, Z(\mathbf{x}, t)]$ describes the random force acting on the DW with $\langle g \rangle = 0$ and $\langle g(\mathbf{x}, z)g(\mathbf{x}', z') \rangle = \delta^d(\mathbf{x} - \mathbf{x}')\Delta_0(z - z')$, with $\Delta_0(z) = \Delta_0(-z)$ being a random force correlator which is a monotonically decreasing function decaying over a finite distance ℓ .

Since the experimental system is a magnetic film, we restrict ourselves to the case $D = 2$ in the following. The dynamics of the system follows from the EW equation of motion:

$$\frac{1}{\gamma} \frac{\partial Z(\mathbf{x}, t)}{\partial t} = - \frac{\delta \mathcal{H}}{\delta Z} + \eta(\mathbf{x}, t), \quad (12)$$

where γ is a kinetic coefficient and $\eta(\mathbf{x}, t)$ a thermal noise term. The DW velocity is given by $v(\mathbf{x}, t) = \dot{Z}(\mathbf{x}, t)$. Here we are interested in the mean DW velocity $v(t) \equiv \langle v(\mathbf{x}, t) \rangle_{\mathbf{x}}$ and mean displacement $Z(t) \equiv \langle Z(\mathbf{x}, t) \rangle_{\mathbf{x}}$, from which we can calculate the ac susceptibility as described above. Here $\langle \dots \rangle_{\mathbf{x}}$ denotes the average over the internal DW coordinate \mathbf{x} .

(i) *adiabatic approach*.— We use the expression for the mean DW velocity in the adiabatic driving regime following from a functional renormalization group (RG) treatment of (12), given in Ref. 45, which interpolates between the creep regime and sliding DW motion,

$$v(H, T) = \begin{cases} \gamma HF(x, y) & \text{for } H \neq 0, \\ 0 & \text{for } H = 0, \end{cases} \quad (13)$$

where $x = H/H_p$, $y = T_p/T$ and

$$F(x, y) = \frac{\Theta(1 - x)}{1 + (yx^{-\mu})^{\beta/\theta}} \exp[yx^{-\mu}(1 - x)^{\theta}] \quad (14)$$

$$+ \Theta(x - 1) \left[\frac{1}{1 + (yx^{-\mu})^{\beta/\theta}} + \left(1 - \frac{1}{x}\right)^{\beta} \right].$$

Here $\Theta(x)$ is the step function, $T_p \simeq \Gamma\ell^2 L_p^{2-d}$ the typical pinning energy on the Larkin length scale L_p , H_p the zero temperature depinning field, and μ , β , and θ the relevant critical exponents⁴⁵ which depend on the DW dimension d . A time discretization, Δt , is used which is chosen to be much smaller than the period of the driving field, $\Delta t = 10^{-5}\mathcal{T}$. Then $Z(t)$ is calculated for each time step by a simple integration of Eq. 13, i.e., $\Delta Z(t_i) = v(H(t_i))\Delta t$, where $v(H(t_i))$ is calculated for each time step from Eq. 13. Here the values of time t , \mathcal{T} , ω , and f are chosen to be dimensionless, since no quantitative comparison to the experiment is required. Formally this can be done by introducing an arbitrary time scale t_0 and substituting $t \rightarrow t/t_0$. Analogously this can be applied to all other parameters and observables, i.e. field $H_0/H_p \rightarrow H_0$, temperature $T/T_p \rightarrow T$, velocity $v \rightarrow v/(\gamma H_p)$ and length, $L_z/L_0 \rightarrow L_z$, where L_0 is an arbitrary length scale.

The magnetization for a finite system is defined here as

$$M(t) = \left(\frac{2Z(t)}{L_z} - 1 \right), \quad (15)$$

where L_z is the extension of the sample in Z -direction and $0 \leq Z \leq L_z$. This implies, that $-1 \leq M \leq +1$. In all cases the initial condition is $Z(0) = L_z/2$. This approach includes the temperature as a parameter, but we restrict our investigations here to small values, $T = 0.1$.

(ii) *non-adiabatic approach*.— Since Eq. (13) was obtained for an adiabatically changing field, it can only be used as an approximation, if the frequency is sufficiently small⁴⁹ (see also Fig. 2 in this Ref.). In order to include the pronounced non-adiabatic effects at higher frequencies (e.g., hysteresis of the velocity), one has to start with the underlying equation of motion (12) which yields

$$\frac{1}{\gamma} \frac{dZ(\mathbf{x}, t)}{dt} = \Gamma \nabla^2 Z(\mathbf{x}, t) + H(t) + g(\mathbf{x}, Z(\mathbf{x}, t)), \quad (16)$$

where the thermal noise term is neglected which is justified since the relaxation times for the DW creep at low temperatures are very long ($\gg \omega^{-1}$) and we consider only finite (not exponentially small) frequencies. In Ref. 49 this equation is studied in detail in the case of an ac driving force in an infinite system and it is shown that thermal effects are not essential for not too low frequencies ($\omega > \omega_T \approx \omega_P(T/T_p)^{\nu z/\theta}$ with the critical exponents ν , z , and θ). Therefore we can restrict ourselves to the zero temperature equation of motion.

In this approach we investigate both infinite ($L_z \rightarrow \infty$) and finite ($L_z < \infty$) systems. In the second case, the DW will hit the boundary of the system for low enough frequencies, such that the magnetization will saturate ($-1 \leq M \leq 1$). Therefore we can derive a critical frequency ω_c above which the system will behave as an infinite system. The finite frequency of the driving force acts as an infrared cutoff for the propagation of the DW which

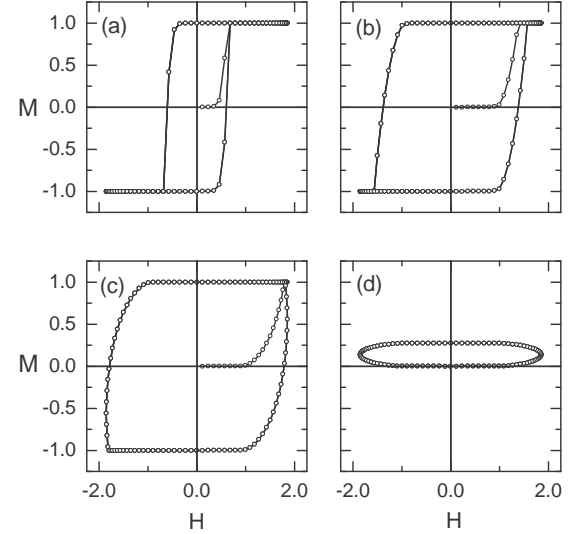


FIG. 2: M vs. H curves from simulations of the adiabatic approach (i) with $T = 0.1$, $H_0 = 1.85$, $L_z = 8.0$, $\mu = 0.24$, $\theta = 0.83$, and $\beta = 0.66$ at different frequencies $f = 1.6 \cdot 10^{-7}$ (a), $1.6 \cdot 10^{-3}$ (b), $7 \cdot 10^{-3}$ (c) and $8 \cdot 10^{-2}$ (d). Note that all quantities are measured in dimensionless units, as described in the text. Lines are guides to the eye.

can move up to a length scale $L_\omega = L_p (\Gamma \gamma L_p^{-2}/\omega)^{1/z}$. Equating this scale to L_z gives the following expression for ω_c (f_c accordingly)

$$\omega_c \approx \omega_p (L_p/L_z)^z, \quad (17)$$

with the typical pinning frequency $\omega_p = \gamma \Gamma / L_p^2$.

For the numerical integration of Eq. (16) it is discretized in \mathbf{x} -direction(s) into N^d positions with a lattice constant α . Here we also go over to dimensionless units with an arbitrary time scale t_0 . These two parameters, α and t_0 , are chosen such that $t_0 \gamma \Gamma / \alpha^2 = 1$ and that the dimensionless random force $t_0 \gamma g$ are set to values in the interval $[-1/2, 1/2]$ at positions with distance ℓ . Between these positions g is interpolated linearly which results in a Gaussian distribution $\Delta_0(z)$ with variance ℓ . The depinning field H_p is not used as input parameter but can be calculated from Eq. (16) (at $\omega = 0$) using a bisection procedure with constant amplitude.

For our simulations we choose $\ell = 0.1$, $N = 1000$, for finite systems $L_z = 8.0$, and a time discretization such that $\Delta t \ll \min(\omega^{-1}, 0.1)$. The results for χ are averaged over 100 disorder configurations for each frequency.

IV. RESULTS AND DISCUSSION

Fig. 2 shows an example of hysteresis loops from simulations within approach (i) with $T = 0.1$, $H_0 = 1.85$ and $L_z = 8.0$ at different frequencies $f = 1.6 \cdot 10^{-7}$ (a), $1.6 \cdot 10^{-3}$ (b), $7 \cdot 10^{-3}$ (c) and $8 \cdot 10^{-2}$ (d). Note that all

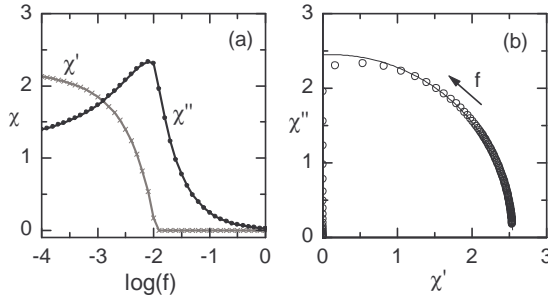


FIG. 3: (a) ac susceptibility, χ' and χ'' vs. ac frequency, f , obtained with model (i) with same parameters as in Fig. 2. (b) Same data, but plotted in the Cole-Cole presentation, χ'' vs. χ' . The solid line represents a least square-fit of the low-frequency data to a circle and the arrow shows in direction of increasing f .

quantities are measured in dimensionless units, as mentioned above. For the values of the critical exponents, we use the results from the RG for $d = 2$, i.e., $\mu = 0.24$ (Ref. 43), $\theta = 0.83$ (Ref. 58), and $\beta = 0.66$ (Ref. 44) (Note, that the precise values of these exponents do not have a significant influence on the behavior under consideration here, especially the qualitative picture does not change if the values are modified slightly.). With increasing frequency, the hysteresis loop broadens until it becomes elliptically shaped above $f = 10^{-2}$ loosing also its inflection symmetry. Similar results are found in experiments.^{31,39}

The ac susceptibility of such hysteresis cycles can be calculated from equations (3) and (4). In Fig. 3 the obtained data is shown for the same set of parameters as for Fig. 2. In (a) one finds the real and imaginary part of the ac susceptibility, χ' and χ'' , as function of the ac frequency. The real part shows an order-parameter like behavior with a non-zero value below and a vanishing value above $f_c \approx 10^{-2}$. Furthermore, the imaginary part has a peak at $f = 8 \cdot 10^{-3} \approx f_c$.

In the Cole-Cole plot, Fig. 3 (b), this transition appears as a sharp change of the slope and curvature. At low frequencies, $f < f_c$ one observes a quarter-circle centered on the χ' -axis. It is possible to fit a circle with the center on the χ' -axis to the low-frequency data (see solid line in (b)). This corresponds well to the experimental result^{31,53} (Fig. 4) and suggest the existence of *one* effective relaxation time in the system. However, for $f > f_c$ only a vertical line can be observed. This result differs from that found in experiment, where the high-frequency part is characterized by a positive slope and positive curvature. This discrepancy needs a closer inspection here.

By comparison of the susceptibility data to the corresponding hysteresis loops (Fig. 2), one sees, that f_c marks the transition between loops saturating at high fields (low-f) and those, which do not saturate (high-f). In the second case the domain wall is always in motion throughout the entire field cycle. The real part is then

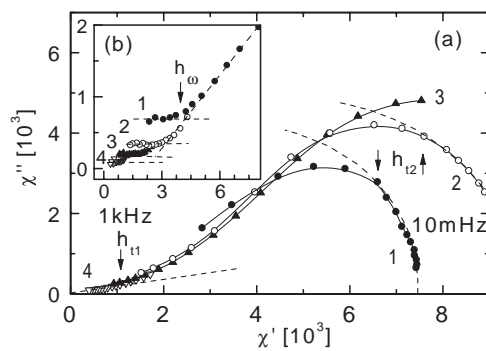


FIG. 4: Experimental Cole-Cole plot taken from Ref. 31 showing χ'' vs. χ' obtained on the SFM granular system [CoFe(1.4nm)/Al₂O₃(2nm)]₁₀. The susceptibility was measured at ac amplitudes $\mu_0 H_0 = 50$ (a) and $5 \mu\text{T}$ (b) at $10 \text{ mHz} \leq f \leq 1 \text{ kHz}$ at $T = 380$ (1), 350 (2), 320 (3) and 260 K (4). Transition fields are marked by arrows³¹.

zero, whereas the imaginary part has a $1/f$ dependence [Fig. 3 (a)], which follows directly from our result shown in Ref. 31, where the complex susceptibility in the case of sliding DW motion is given by $\tilde{\chi} = \chi_\infty [1 + 1/(i\omega\tau)]$, or more generally by $\tilde{\chi} = \chi'_\infty + \chi''_\infty/(i\omega\tau)$. For $\chi'_\infty = 0$ this yields directly the vertical part in the Cole-Cole plot [Fig. 3 (b)]. In Ref. 31 was argued, that the non-linearity of the $v(H)$ function in the creep regime can be taken into account by introducing a polydispersivity exponent, β , in the above equation, $\tilde{\chi} = \chi_\infty [1 + 1/(i\omega\tau)^\beta]$ (compare to a similar relationship formulated for the conductivity of disordered hopping conductors $\sigma(\omega) \sim (-i\omega\tau)^\nu(T)$, where $0 < \nu < 1$)^{59,60}. This yields the linear relationship, $\chi'' = \tan(\pi\beta/2)[\chi' - \chi_\infty]$. Note, that for *any* velocity function $v = v(H)$ with $v(H) = -v(-H)$ and without velocity hysteresis⁴⁹ it follows, that $\chi' = 0$ and $\chi'' \propto 1/f$.⁵⁰ This can easily be seen from Eqs. (5) and (6) and $M \propto v$. The consequence is that a monotonically increasing part with finite slope cannot be found in the Cole-Cole plot by considering only the adiabatic motion of one DW.

There are two possible ways to improve the model. The first one is to simulate an ensemble of non-interacting subsystems with different domain propagations lengths, pinning fields, H_p , or depinning energies, T_p . It is possible, that this case would yield the situation above qualitatively described by the polydispersivity exponent $\beta < 1$. The second is to employ a more realistic description of the DW by using the above introduced non-adiabatic approach (ii). The latter case was studied here.

In Fig. 5 the results for the magnetization hysteresis of a DW from Eq. 16 for $H_0 = 1.85$ are presented. The plots (a) to (c) show hysteresis loops at different frequencies, $f = 0.0016$ (a), 0.08 (b), and 0.48 (c) for an infinite system ($L_z \rightarrow \infty$). Here we define $M = Z$. In this case the DW never touches the sample boundary. At low frequencies one finds a symmetric loop with respect

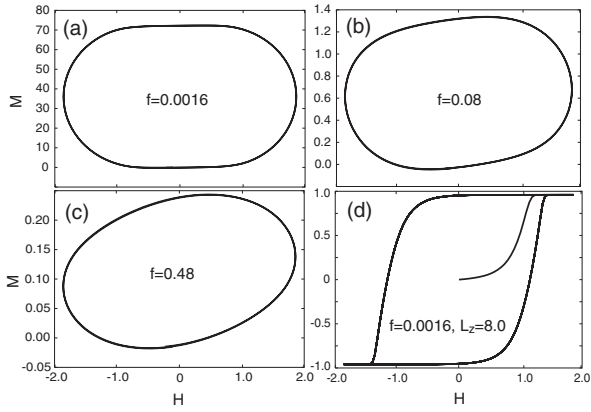


FIG. 5: M vs. H curves for the non-adiabatic approach (ii) with $H_0 = 1.85$ at different frequencies, $f = 0.0016$ (a), 0.08 (b), and 0.48 (c) for an infinite system (in this case one defines $M = Z$). (d) shows the magnetization curve for $f = 0.0016$ but a finite system ($L_z = 8.0$) so that the DW touches the boundaries.

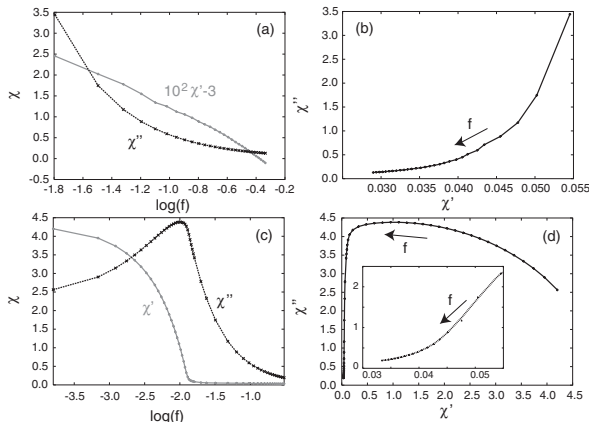


FIG. 6: Real and Imaginary part of the ac susceptibility vs. frequency, calculated within approach (ii) for infinite systems (a) [the real part is shifted and scaled] and the corresponding Cole-Cole plot (b). In (c) χ' and χ'' are plotted for the finite system ($L_z = 8.0$) and Cole-Cole plot (d). The inset in (d) shows the high frequency behavior in more detail. The arrows show in direction of increasing frequencies. All simulations were performed with $H_0 = 1.85$.

to the M axis (a) similar to the result shown above in Fig. 2(d). This symmetry is lost upon increasing the frequency, (b) and (c), and the loop becomes tilted. This tilting is responsible for a non-vanishing real part of the ac susceptibility and cannot be observed in approach (i). The tilting corresponds to the appearance of a velocity hysteresis.⁴⁹ That means there exists no functional relationship between the velocity and the field any more, as it is the case in the adiabatic regime.

The resulting susceptibilities are plotted in Fig. 6. In (a) and (b) the real and imaginary part vs. $\log(f)$ and the corresponding Cole-Cole plot, respectively, are shown for an infinite system, when the DW never touches the

boundary. In (c) and (d) the same plots are shown for a finite system ($L_z = 8.0$). While the low-frequency parts resemble those from approach (i), the high-frequency part shows a completely different behavior. For $\chi' \rightarrow 0$ we find in the Cole-Cole plot [inset in Fig. 6 (d)] a curve with positive curvature similar as in the experiment (Fig. 4). One can expect that χ goes to 0 with $\omega \rightarrow \infty$, since the velocity hysteresis disappears for $\omega \rightarrow \infty$. Obviously the more realistic second model is capable to describe the experimentally found behavior. At this point we want to emphasize that the adiabatic approach only works for low frequencies, where non-adiabatic effects can be neglected. Furthermore it only works at finite temperatures. On the other hand the non-adiabatic approach can explain the main experimental features even if we use the zero temperature equation of motion, since the smearing effects of the depinning transition due to finite frequencies dominate the thermal creep effects at low temperatures.

However, two drawbacks still exist. One, the Cole-Cole plot from the simulation shows a rather steep and narrow increasing part compared to the experiment. Second, we cannot retrieve the experimentally observed saturating part for the highest experimental frequencies, where the imaginary part becomes constant (see Fig. 4, inset). This case was attributed³¹ to the reversible relaxation response of the DW for high frequencies and small excitations fields.^{50,58} It would be interesting to study this case with a suitably modified model which includes multiple and interacting DWs.

V. CONCLUSION

In order to get a better understanding of the magnetic behavior found in the superferromagnetic granular multilayer [$\text{Co}_{80}\text{Fe}_{20}(1.4\text{nm})/\text{Al}_2\text{O}_3(3\text{nm})]_{10}$ we employed two types of simulations of a domain wall in random media driven by an external magnetic field. Using the first approach with the mean velocity of a domain wall in the adiabatic limit, one can explain the monodisperse dynamic response evidenced by a partial semicircle centered around the χ' axis. However, it fails to describe the increasing part with positive curvature for higher frequencies in the Cole-Cole plot. This behavior can be found by taking the full equation of motion into account, where an elastic interface is driven in general *non-adiabatically* in a random medium. Hence a model of an impure ferromagnet is capable to describe the main features of the experimental results. We find that the appearance of a velocity hysteresis is a crucial element in the dynamic response of the superferromagnet. We show that a Cole-Cole plot may be used to classify magnetic systems by their dynamic response. E.g. the above mentioned granular superferromagnet can unambiguously be distinguished from a superparamagnet and a superspin glass system.

Acknowledgments

We thank Ch. Binek and X. Chen for helpful discussions. This work has been supported by the Alexander-

von-Humboldt Foundation (O.P.) and the Deutscher Akademischer Austauschdienst (A.G.).

^{*} e-mail:opetr@kleemann.uni-duisburg.de
[†] e-mail:ang@thp.uni-koeln.de

¹ J. L. Dormann, D. Fiorani, and E. Tronc, *Adv. Chem. Phys.* **98**, 283 (1997).
² V. F. Puntes, K. M. Krishnan, and A. P. Alivisatos, *Science* **291**, 2115 (2001), and References therein.
³ X. Batlle and A. Labarta, *J. Phys. D: Appl. Phys.* **35**, R15 (2002).
⁴ C. Djurberg, P. Svedlindh, P. Nordblad, M. F. Hansen, F. Boedker, and S. Moerup, *Phys. Rev. Lett.* **79**, 5154 (1997).
⁵ S. I. Woods, J. R. Kirtley, S. Sun, and R. H. Koch, *Phys. Rev. Lett.* **87**, 137205 (2001).
⁶ F. Luis, F. Petroff, J. M. Torres, L. M. García, J. Bartolomé, J. Carrey, and A. Vaures, *Phys. Rev. Lett.* **88**, 217205 (2002).
⁷ S. Sahoo, O. Petracic, W. Kleemann, S. Stappert, G. Dumpich, P. Nordblad, S. Cardoso, and P. P. Freitas, *Appl. Phys. Lett.* **82**, 4116 (2003).
⁸ J.-O. Andersson, C. Djurberg, T. Jonsson, P. Svedlindh, and P. Nordblad, *Phys. Rev. B* **56**, 13983 (1997).
⁹ M. Ulrich, J. García-Otero, J. Rivas, and A. Bunde, *Phys. Rev. B* **67**, 024416 (2003).
¹⁰ P. J. Jensen and G. M. Pastor, *New J. Phys.* **5**, 68.1 (2003).
¹¹ M. Porto, *Eur. Phys. J. B* **26**, 229 (2002).
¹² D. Kechrakos and K. N. Trohidou, *Phys. Rev. B* **58**, 12169 (1998).
¹³ L. Néel, *Ann. Geophys.* **5**, 99 (1949).
¹⁴ W. F. Brown, Jr, *Phys. Rev.* **130**, 1677 (1963).
¹⁵ J. L. García-Palacios, *Adv. Chem. Phys.* **112**, 1 (2000), and References therein.
¹⁶ P. Polit and M. G. Pini, *Phys. Rev. B* **66**, 214414 (2002).
¹⁷ V. Russier, *J. Appl. Phys.* **89**, 1287 (2001).
¹⁸ V. N. Kondratyev and H. O. Lutz, *Phys. Rev. Lett.* **81**, 4508 (1998).
¹⁹ R. V. Chamberlin, J. Hemberger, A. Loidl, K. D. Humfeld, D. Farrell, S. Yamamoto, Y. Ijiri, and S. A. Majetich, *Phys. Rev. B* **66**, 172403 (2002).
²⁰ J. L. Dormann, R. Cherkaoui, L. Spinu, M. Nogues, F. Lucari, F. D’Orazio, D. Fiorani, A. Garcia, E. Tronc, and J. P. Jolivet, *J. Magn. Magn. Mater.* **187**, L139 (1998).
²¹ P. E. Joensson and J. L. García-Palacios, *Phys. Rev. B* **64**, 174416 (2001).
²² H. Mamiya, I. Nakatani, and T. Furubayashi, *Phys. Rev. Lett.* **82**, 4332 (1999).
²³ M. G. del Muro, X. Batlle, and A. Labarta, *Phys. Rev. B* **59**, 13584 (1999).
²⁴ S. Sahoo, O. Petracic, W. Kleemann, P. Nordblad, S. Cardoso, and P. P. Freitas, *Phys. Rev. B* **67**, 214422 (2003).
²⁵ S. Moerup, M. B. Madsen, J. Franck, J. Villadsen, and C. J. W. Koch, *J. Magn. Magn. Mater.* **40**, 163 (1983).
²⁶ J. Hauschild, H. J. Elmers, and U. Gradmann, *Phys. Rev. B* **57**, 677 (1998).
²⁷ M. R. Scheinfein, K. E. Schmidt, K. R. Heim, and G. G. Hembree, *Phys. Rev. Lett.* **76**, 1541 (1996).
²⁸ W. Kleemann, O. Petracic, C. Binek, G. N. Kakazei, Y. G. Pogorelov, J. B. Sousa, S. Cardoso, and P. P. Freitas, *Phys. Rev. B* **63**, 134423 (2001).
²⁹ V. F. Puntes, P. Gorostiza, D. M. Aruguete, N. G. Bastus, and A. P. Alivisatos, *Nature materials* **3**, 263 (2004).
³⁰ A. F. Bakuzis and P. Morais, *J. Magn. Magn. Mater.* **in print** (2004).
³¹ X. Chen, O. Sichelschmidt, W. Kleemann, O. Petracic, C. Binek, J. B. Sousa, S. Cardoso, and P. P. Freitas, *Phys. Rev. Lett.* **89**, 137203 (2002).
³² C. Binns, M. J. Maher, Q. A. Pankhurst, D. Kechrakos, and K. N. Trohidou, *Phys. Rev. B* **66**, 184413 (2002).
³³ J. F. Loeffler, H.-B. Braun, and W. Wagner, *Phys. Rev. Lett.* **85**, 1990 (2000).
³⁴ R. H. Kodama, A. E. Berkowitz, J. E. J. McNiff, and S. Foner, *Phys. Rev. Lett.* **77**, 394 (1996).
³⁵ B. Raquet, R. Mamy, and J. C. Ousset, *Phys. Rev. B* **54**, 4128 (1996).
³⁶ W. Y. Lee, B.-C. Choi, Y. B. Xu, and J. A. C. Bland, *Phys. Rev. B* **60**, 10216 (1999).
³⁷ H.-T. Wang and S. T. Chui, *Phys. Rev. B* **60**, 12219 (1999).
³⁸ I. F. Lyuksyutov, T. Nattermann, and V. Pokrovsky, *Phys. Rev. B* **59**, 4260 (1999).
³⁹ I. Ruiz-Feal, T. A. Moore, L. Lopez-Diaz, and J. A. C. Bland, *Phys. Rev. B* **65**, 054409 (2002).
⁴⁰ S. Chikazumi, *Physics of Ferromagnetism Second Edition* (Clarendon Press, 1997).
⁴¹ M. V. Feigelman, V. B. Geshkenbein, A. I. Larkin, and V. M. Vinokur, *Phys. Rev. Lett.* **63**, 2303 (1989).
⁴² P. Chauve, T. Giamarchi, and P. Le Doussal, *Phys. Rev. B* **62**, 6241 (2000).
⁴³ S. Lemerle, J. Ferré, C. Chappert, V. Mathet, T. Giamarchi, and P. Le Doussal, *Phys. Rev. Lett.* **80**, 849 (1997).
⁴⁴ L. Roters, A. Hucht, S. Luebeck, U. Nowak, and K. D. Usadel, *Phys. Rev. E* **60**, 5202 (1999).
⁴⁵ T. Nattermann, V. Pokrovsky, and V. M. Vinokur, *Phys. Rev. Lett.* **87**, 197005 (2001).
⁴⁶ R. Cowburn, J. Ferré, S. J. Gray, and J. A. C. Bland, *Appl. Phys. Lett.* **74**, 1018 (1999).
⁴⁷ H. Jang, M. J. Grimson, and C. K. Hall, *Phys. Rev. B* **67**, 094411 (2003).
⁴⁸ D.-X. Chen, V. Skumryev, and J. M. D. Coey, *Phys. Rev. B* **53**, 15014 (1996).
⁴⁹ A. Glatz, T. Nattermann, and V. Pokrovsky, *Phys. Rev. Lett.* **90**, 047201 (2003).
⁵⁰ A. A. Fedorenko, V. Mueller, and S. Stepanow, arXiv:cond-mat/0406401 (2004).
⁵¹ S. F. Edwards and D. Wilkinson, *Proc. R. Soc. London Ser. A* **381**, 17 (1982).
⁵² E. Fatuzzo, *Phys. Rev.* **127**, 1999 (1962).
⁵³ O. Petracic, X. Chen, O. Sichelschmidt, C. Binek, W. Kleemann, A. Glatz, T. Nattermann, S. Cardoso, and P. P. Freitas, *J. Magn. Magn. Mater.* **272-276**, E1201 (2004).
⁵⁴ K. S. Cole and R. H. Cole, *J. Chem. Phys.* **9**, 341 (1941).
⁵⁵ A. K. Jonscher, *Dielectric Relaxation in Solids* (Chelsea

Dielectrics Press, London, 1983).

⁵⁶ J. Mydosh, *Spin Glasses : An Experimental Introduction* (Taylor and Francis, London, 1993).

⁵⁷ O. Petracic, S. Sahoo, C. Binek, W. Kleemann, J. B. Sousa, S. Cardoso, and P. P. Freitas, Phase Transit. **76**, 367 (2003).

⁵⁸ T. Nattermann, Y. Shapir, and I. Vilfan, Phys. Rev. B **42**, 8577 (1990).

⁵⁹ J. Bernasconi, H. Beyeler, and S. Straessler, Phys. Rev. Lett. **42**, 819 (1979).

⁶⁰ T. Ishii, Prog. Theor. Phys. **73**, 1084 (1985).

⁶¹ $(\sqrt{2}V^2/\sqrt{\pi})(\Delta V)^3 \exp[-V^2/2(\Delta V)^2]$.